Toward Using Monostatic Antennas with Near-Field Cancellation Technique in IBFD Phased Arrays

Hanan Ouled Angoura, Hadi Hijazi, Ulrich B. Y. Simpore, Marc Le Roy, Jean-Thierry Kubwimana, Raafat Lababidi, Roland Gautier, Stephane Mallegol, Gérard Tanné, André Pérennec

Toward Using Monostatic Antennas with Near-Field Cancellation Technique in IBFD Phased Arrays

Hanan Ouled Angoura[1*], Hadi Hijazi[2] , Ulrich B. Y. Simpore [1] , Marc Le Roy[1], Jean-Thierry Kubwimana[1],
Raafat Lababidi[2], Roland Gautier[1], Stéphane Mallegol[3], Gerard Tanne[1], André Pérennec[1]
[1]Univ Brest , [2]ENSTA Bretagne,[3]Thales DMS, Lab-STICC, CNRS, UMR 6285, F-29200 Brest
* hanan.ouledangoura@univ-brest.fr

***Abstract*— This paper presents an S-Band monostatic 2x2 patch array, with shared radiating elements among Tx and Rx, for In-Band Full-Duplex (IBFD) applications. In this array, self-interference cancellation (SIC) is achieved by locally implementing the near field cancellation (NFC) technique at each single patch by a multi-point differential feeding, which also ensures global SIC at the array level. Moreover, to identify the major coupling paths between array ports that contribute to cancellation, we provide some coupling matrices as a new way to represent the magnitude and phase combinations of inter- and intra-port coupling. In addition to that, we demonstrate the variation of cancellation level as the Tx and Rx beams are steered independently.**

Keywords*— Coupling Matrix, In-Band Full-Duplex, Phased Array, S-Band, Self-Interference Cancellation, Simultaneous Transmit and Receive.

I. Introduction

Simultaneously transmitting and receiving a wireless signal at the same frequency, has been identified as an attractive way to alleviate spectrum resources scarcity [1]. This is achieved by tending toward the potential double spectral efficiency promised by IBFD compared to current techniques. Moreover, IBFD also brings opportunities for simultaneous multi-function front-end antenna systems in the electronic warfare domain [2]. The primary challenge of IBFD is Self-Interference (SI), leaking from the transmitter to its own co-localized receiver [3]. Most systems require a very high level of Self-Interference Cancellation (SIC) to operate properly. Generally, to achieve the expected 110-130 dB of SIC, cancellation is implemented, as shown in Fig. 1, at three levels: RF or antenna, analog, and digital [4]-[5].

The analog cancellation stage targets re-building an opposite (anti-phase) signal that mimics the SI signal at the Rx stages [4]. This canceller architecture requires numerous delay/phase-shifting cells and attenuators resulting in a complex, sensible, and narrow-band parallel path. Moreover, this complexity and sensibility is greatly increased in antenna arrays that require numerous parallel cancellation networks. Therefore, to get rid of this complex and weakly reconfigurable analog stage, we need to search for a combination of 50-60 dB of SIC at the antenna level with another 50-60 dB of SIC from an environment-adaptive digital SIC stage [5], as illustrated in Fig. 1. Getting a high level of SIC at the antenna level prevents deterioration in the performance of the Rx devices, particularly the LNA, mixer, and ADC. It also avoids all the non-linear and phase noise components introduced along the Tx chain.

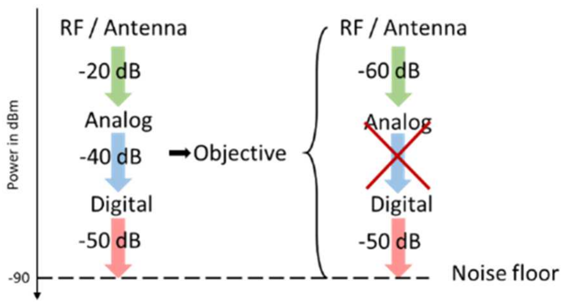

Fig. 1.Illustration of total SIC obtained by multi-level SIC techniques

To mitigate self-interference at the antenna level, different techniques have been introduced in the literature [6]-[7] (Fig.2), and they can be categorized as bi-static, where separate antennas are used for Tx and Rx, or monostatic where the radiating elements are shared between Tx and Rx. Among the available techniques, Near-Field Cancellation (NFC) can be applied to both categories achieving a high isolation level over a potentially wide bandwidth. Moreover, NFC can be combined with other techniques such as polarization and directional diversity to increase the SIC level.

In monostatic configurations with separate antenna-feeding points, SIC is more challenging than in bistatic topologies due to the closer distance between Tx and Rx ports, resulting in a higher coupling level. As compared to its bistatic counterpart, the monostatic NFC has a better gain/surface ratio and thus can help reduce the level of grating lobes at broadside in arrays [8]. This technique involves placing and feeding the Tx ports oppositely to achieve NFC along the Rx axis [6]-[7]. The same principle applies to the Rx part allowing the cancellation of residual SI and enabling optimal phase recombination of far-field radiation patterns.

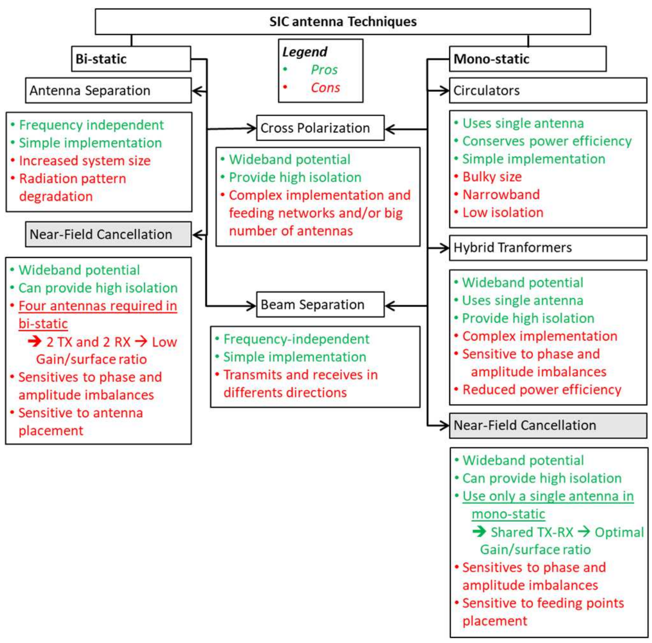

Fig. 2. SIC techniques at the antenna level

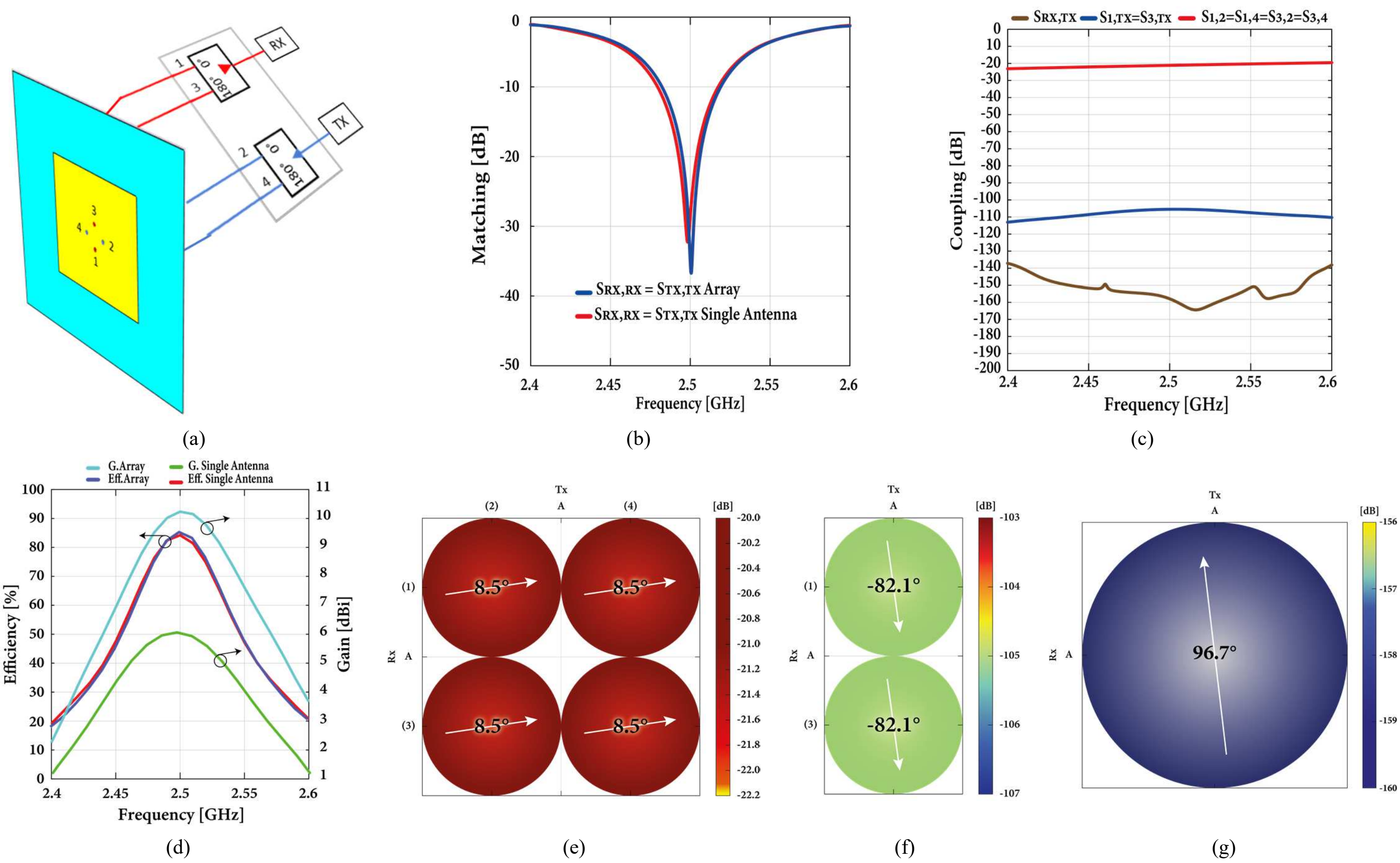

Fig. 3. (a) IBFD antenna, system (b) matching, (c) port coupling, (d) efficiency & gain, (e) coupling matrix of antenna ports, (f) coupling matrix from Tx-balun to antenna Rx ports, (g) coupling matrix between Tx-balun and Rx balun.

In a monostatic IBFD array implementation, it's of paramount interest to identify both the critical coupling paths and the mechanisms of cancellation. This can provide some useful information and tools to further optimize the beamsteering and beamforming algorithms to guarantee or improve the SIC level in the array. Therefore, in this paper, we present an original representation of several coupling matrices at different stages of the antenna system to better visualize, step by step, how the NFC technique operates.

This paper is organized as follows: section II presents a monostatic IBFD system consisting of a 4-port differently fed single patch antenna using NFC. Based on that, a 2x2 array is detailed in section III along with its coupling matrices and performance. Also, the variation of SIC with beam steering is discussed in section IV. And finally, a conclusion is drawn in section V.

II. Single 4-port Monostatic antenna

Fig. 3(a) shows the schematic of a 4-port differently fed patch antenna based on NFC. The ports are placed following a 90° sequential rotation around the center of the patch. Two ports are dedicated to Tx and the other two for Rx, and each pair is connected to an external balun. Hence, the input signals at each pair of opposite ports have identical amplitudes and a 180° phase difference. In this case, the Tx signals are canceled in near-field along the Rx axis and recombined in far-field.

This patch antenna was simulated in CST microwave studio (time-domain solver) on a RO4003C substrate having ε_r = 3.55 and h = 1.524 mm. The patch is square-shaped with a side length of 30.5 mm and is fed by four coaxial probes with PTFE insulation having an inner diameter of 0.6 mm and an outer diameter of 2 mm.

The main RF characteristics of the antenna are plotted in Fig. 3(b)-(d) using ideal baluns. The matching level (red curve in Fig. 3(b)) at 2.5 GHz is better than 30 dB, and the global Tx-Rx coupling level (brown curve in Fig. 3(c)) is 158 dB. Moreover, the antenna efficiency exceeds 84% and its co-polarized broadside gain is 6 dBi. However, with real components, we may expect the cancellation level to be much lower, primarily because the measurements will likely exhibit phase and amplitude imbalances between the output signals of the baluns. These imbalances can significantly impact the level of the achieved cancellation [6].

An antenna array can be built based on this configuration, however, as the number of the array elements increases, it becomes more complex to plot and analyze all S-parameters. Therefore, we introduce the coupling matrices in Fig. 3(e)-(g) as a more effective way of visualizing the complex interactions between different antenna ports, thereby facilitating the analysis and interpretation of the results obtained. All these matrices are plotted in Matlab using the S-parameters obtained from CST Microwave Studio simulations of the single antenna or the array. These matrices help identify the mechanisms of coupling/decoupling between the ports of each antenna and between the array elements. Therefore, this approach aids in managing the SIC

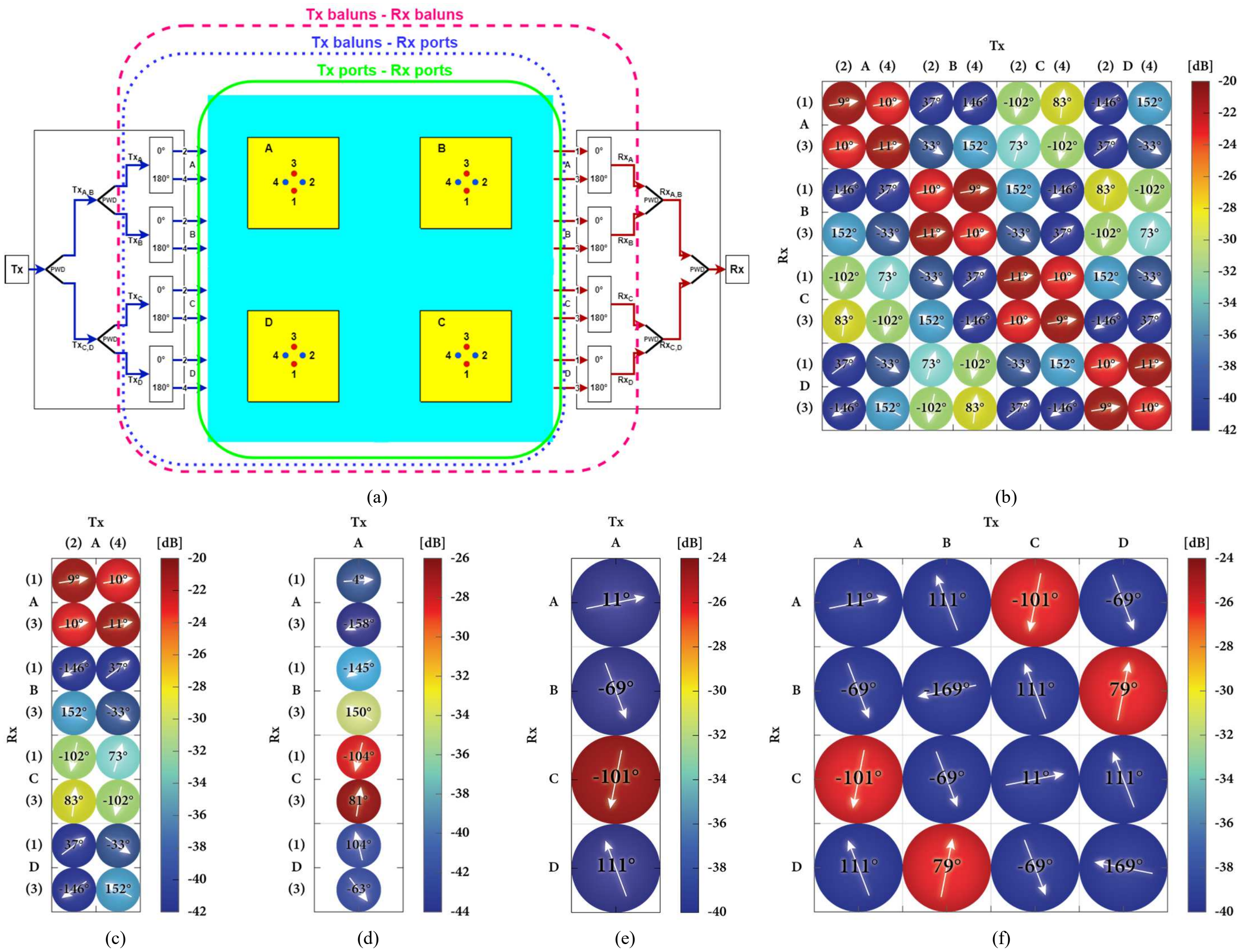

Fig. 4. (a) IBFD array, (b) coupling matrix from antennas Tx ports to antennas Rx ports, (c) coupling matrix from antenna A Tx ports to all antennas Rx ports, (d) coupling matrix from Tx balun of antenna A to all antennas Rx ports, (e) coupling matrix from antenna A Tx balun to all Rx baluns (f) coupling matrix from Tx baluns to Rx baluns

at the array level or sub-array level and introducing further improvements or optimization steps.

The matrix plotted in Figure 3(e) shows the coupling between the antenna's Tx and Rx ports without any balun. The coupling level is between -22 and -20 dB and the phases (from EM-simulated S-parameters) are identical, as indicated by the numbers and the arrows. After that, Fig. 3(f) illustrates the effect of adding a balun at Tx ports on the Rx ports, where the coupling drops to less than -105 dB, while the phases remain synchronized. Finally, Fig. 3(g) shows that when baluns are applied to both Tx and Rx ports, the remaining couplings recombine and cancel out each other, resulting in an overall cancellation better than 158 dB.

III. 2X2 MONOSTATIC ARRAY PERFORMANCE

The array configuration of Fig. 4(a) consists of 4 square patch antennas each connected to two ideal baluns: the balun in blue connects to the Tx ports, while the one in red connects to the Rx ports. Then all the Tx baluns are combined using a 3 dB power divider. And the same applies to Rx baluns. This allows canceling the transmitted signal in near-field and recombining it in far-field. As in section II, the single intra-antenna SI will be visualized through the coupling matrices but also the array inter-element coupling to identify the main SI contributions and the step-by-step SIC mechanisms in an ideal configuration.

The main RF characteristics of the antenna array are also plotted in Fig. 3(b) and 3(d). It is evident that the network achieves very good matching at the central frequency (2.5 GHz), with a value lower than -35 dB. Also, the efficiency exceeds 84% and the co-polarized gain surpasses 10.30 dBi.

The coupling matrix between all ports of the array without having a balun neither at Tx nor Rx is plotted in Fig. 4(b) which corresponds to the area delimited by the green line in Fig. 4(a). If we consider the first column of this matrix, which is plotted in Fig. 4(c), we can distinguish three levels of coupling between the array ports:

1. The first and strongest level is the coupling between the Tx and Rx ports of the same patch, identifiable by the red color, with values ranging from -20 dB to -26 dB.
2. The second level corresponds to the coupling between the diagonally opposite antennas, for example between A and C, with values ranging from -26 to -36 dB.

3. Finally, the third level involves the coupling between antennas located on the same horizontal or vertical axis, with values ranging from -36 to -42 dB.

Next, for each patch antenna, a single balun is connected to its Tx ports (i.e. inside the area delimited by the blue dot line in Fig4(a)). And the matrix in Fig. 4(d) represents the coupling between each individual Tx balun and all Rx ports.

1. The coupling between the Tx balun and Rx ports of the same patch has been reduced to a level between -39 and -44 dB (first two rows in Fig. 4(c) and (d)) as evidenced from single antenna analysis but with a lower decrease due to the influence of adjacent patches that degrades the E-field distribution symmetry on the patch.
2. The coupling between the Tx balun and Rx ports of the diagonally opposite antennas has increased to range from -26 to -30 dB (e.g. rows 5 and 6 in Fig. 4(c) and (d)). This increase is a result of the constructive combination of the coupling phase vectors which had near-opposite phase values before adding the Tx baluns and became near-identical after adding the baluns. This indicates that adding a balun at the Tx ports of a single antenna is not sufficient to cancel the coupling between the Tx of this antenna and the Rx of the other antennas.
3. The level of coupling between the Tx balun and the Rx ports of the vertically or the horizontally adjacent antennas might increase or decrease depending on their phase vectors as explained above.

In the final step (i.e. delimited by the pink dot line in Fig.4(a)), a balun is also connected to the Rx ports of each antenna, and the coupling matrix is plotted in Fig. 4(e) for the first column and Fig. 4(f) between all the baluns ports. It is observed that, in general, the value of coupling between the Tx and Rx baluns also increases depending on their phase vectors. This indicates that implementing NFC at the single antenna level is not sufficient to cancel the coupling between the Tx of one antenna and the Rx of the other antennas.

The matrix in Fig. 4(f) shows that, at the array level, the coupling between the vertically and horizontally symmetrical patches now have identical amplitudes and opposite phases (for example, coupling from A to D and from A to B). Therefore, they will combine destructively at the array level after combining the baluns using power dividers. The same applies to the diagonally opposite antennas (coupling from A to D cancels coupling from B to D). Finally, by feeding the Tx baluns inputs through a power divider and recombining the Rx baluns output by a power combiner the global theoretical cancellation at the antenna array level is 157 dB.

IV. SIC for independent Tx and Rx elevation angles

In the context of applying beam steering to an IBFD array, especially where independent steering for Tx and Rx is desired, it's important to estimate the variation of SIC as the steering angle changes. Therefore, in this article, we study this variation for the previous array assuming only 1D beam steering (only in elevation) for both Tx and Rx. Fig. 5 shows the variation of coupling as a function of steering in elevation (θ_{Tx},θ_{Rx}) for the 2x2 array in the steering range from -45° to 45°. It is observed that the maximum cancellation is obtained when one of the beams is fixed at 0° and the other is steered, and this value starts to decrease (but remains low) when both beams are steered at the same time. This is mainly due to the asymmetric phase distribution of the Tx and Rx signals that becomes scrambled with the simultaneous steering.

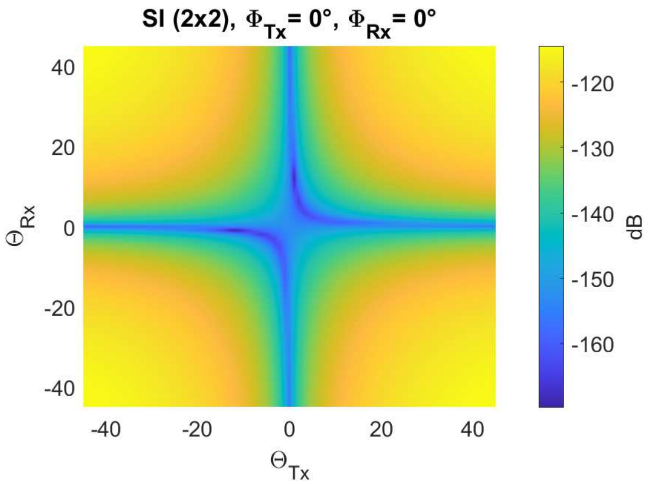

Fig. 5. SI level as a function of steering in elevation from -45° to 45°.

V. Conclusion

In summary, this paper presents an S-Band 2x2 patch antenna array with In-Band Full-Duplex capabilities for beam steering applications. The proposed array utilizes the Near-Field Cancellation technique to achieve a simulated level of SIC higher than 157 dB. The array is well matched at the central frequency of 2.5 GHz, and it can achieve a gain higher than 10.3 dBi and an efficiency surpassing 84%. The analysis of the coupling between different elements of the array was made easier by providing coupling matrices which is a more effective way of visualizing the complex interactions between different antenna ports, thereby facilitating the analysis and interpretation of the results obtained. Simulations are currently underway to anticipate the SIC degradations coming from phase and magnitude imbalances (e.g. introducing ±0.2dB and 0.8° of imbalance as currently present in off-the-shelf baluns/transformers) while steering independently the Tx and Rx beams.

Aknowledgements

This work was supported in part by Thales DMS France through a GIS cormorant project and also in part by "FullSSAT" ASTRID project funded by DGA/AID.

References

[1] Z. H. Hong, L. Zhang, Y. Wu, W. Li, SI. Park, S. Ahn, N. Hur, E. Iradier, J. Montalban, P. Anguiera, « Iterative Successive Nonlinear Self-Interference Cancellation for In-Band Full-Duplex Communications », IEEE Trans. on Broadcasting, vol. 70, no. 1, pp. 2-13, March 2024.

[2] K. Pärlin, T. Riihonen, V. Le Nir, M. Bowyer, T. Ranstrom, E. Axell, B. Asp, R. Ulman, M. Tschauner, M. Adrat, « Full-Duplex Tactical Information and Electronic Warfare Systems », IEEE Communications Magazine, vol. 59, nº 8, p. 73-79, 2021.

[3] A. Sabharwal, P. Schinter, D. Guo, D. W. Bliss, S. Rangarajan, R. Wichman, « In-Band Full-Duplex Wireless: Challenges and Opportunities », IEEE J. Select. Areas Commun., vol. 32, nº 9, p. 1637-1652, 2014.

[4] M. Chung, M. S. Sim, J. Kim, D. K. Kim, C. Chae, « Prototyping real-time full duplex radios », IEEE Communications Magazine, vol. 53, no. 9, pp. 56-63, September 2015.

[5] J. Kim, H. Lee, H. Do, J. Choi, J. Park, W. Shin, C. Eldar, N. Lee, « On the Learning of Digital Self-Interference Cancellation in Full-Duplex Radios », IEEE Wireless Communications, vol. 31, no. 4, pp. 184-191, August 2024.

[6] H. Hijazi, M. Le Roy, R. Lababidi, D. Le Jeune, A. Pérennec, «Ultra-wideband antenna system for in‐band full‐duplex applications. » IET Microwaves, Antennas & Propagation, HIJAZI, Hadi, LE ROY, Marc, LABABIDI, Raafat, et al. Ultra‐wideband antenna system for in‐band full‐duplex applications. IET Microwaves, Antennas & Propagation, no.15, p. 1853-1865. 2021.

[7] K. E. Kolodziej, B. T. Perry, J. S. Herd, « In-Band Full-Duplex Technology: Techniques and Systems Survey », IEEE Transactions on Microwave Theory and Techniques, vol. 67, no. 7, pp. 3025-3041, July 2019.

[8] H. Hijazi, M. Le Roy, R. Lababidi, D. Le Jeune, A. Pérennec, « Ultra-wideband 3D-printed vivaldi array for in-band full-duplex applications with a grating lobes reduction approach », AEU-International Journal of Electronics and Communications, vol. 171, 2023.